Matrix-Bound Nanovesicle-Mediated Immunomodulation to Protect and Repair Injured Retina and Optic Nerve

Pitt McGowan

University of Pittsburgh

Peyton M Leyendecker[1,2], Scott A Johnson[1,3], Catalina Pineda Molina[1,3], Ethan A Rossi[1,2,4], George S Hussey[1,2,3,5]

[1]McGowan Institute for Regenerative Medicine, University of Pittsburgh, Pittsburgh, PA. [2]Department of Bioengineering, Swanson School of Engineering, University of Pittsburgh, Pittsburgh, PA. [3]Department of Surgery, School of Medicine, University of Pittsburgh, Pittsburgh, PA. [4]Department of Ophthalmology, School of Medicine, University of Pittsburgh, Pittsburgh, PA. [5]Department of Pathology, School of Medicine, University of Pittsburgh, Pittsburgh, PA.

INTRODUCTION

Traumatic retinal and optic nerve injury is a leading cause of irreversible battlefield vision loss. In austere combat settings, evacuation to a vitreoretinal microsurgeon can take up to five days. During this window, secondary pro-inflammatory injury cascades often inflict more damage than the initial trauma. Currently, no therapy bridges this gap.

Closing this gap requires two things: a validated large-animal model that reproduces this specific combat-relevant injury, and a portable therapy that can be delivered within it. This study addresses both, establishing a model of acute ocular hypertension, while using it to test matrix-bound nanovesicles (MBVs) as a candidate for treatment.

What are Matrix-Bound Nanovesicles (MBVs)?

MBVs are naturally occurring extracellular vesicles (EVs) tightly bound within the native extracellular matrix (ECM). MBVs carry a distinct cargo of regulatory proteins and microRNA that modulate pro-inflammatory immune activation and support tissue repair. Additionally, MBVs can be purified from decellularized ECM into a stable, room-temperature, off-the-shelf biologic, making them uniquely suited for delivery in less-than-ideal conditions. This study evaluated clinical-grade MBVs manufactured under current good manufacturing practice (cGMP) specifications at ECM Therapeutics, Inc.

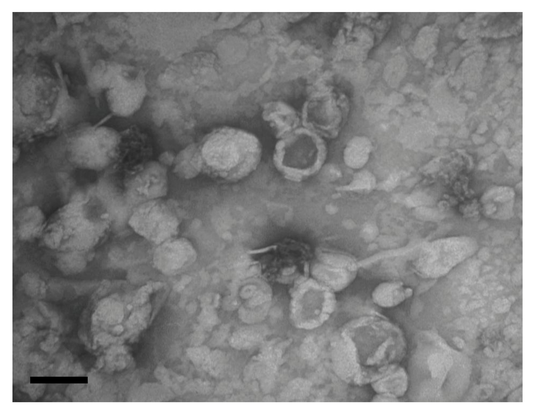

Fig. 1. Transmission electron micrograph of purified MBVs. Negatively stained with uranyl acetate. Scale bar 100 nm.

METHODS

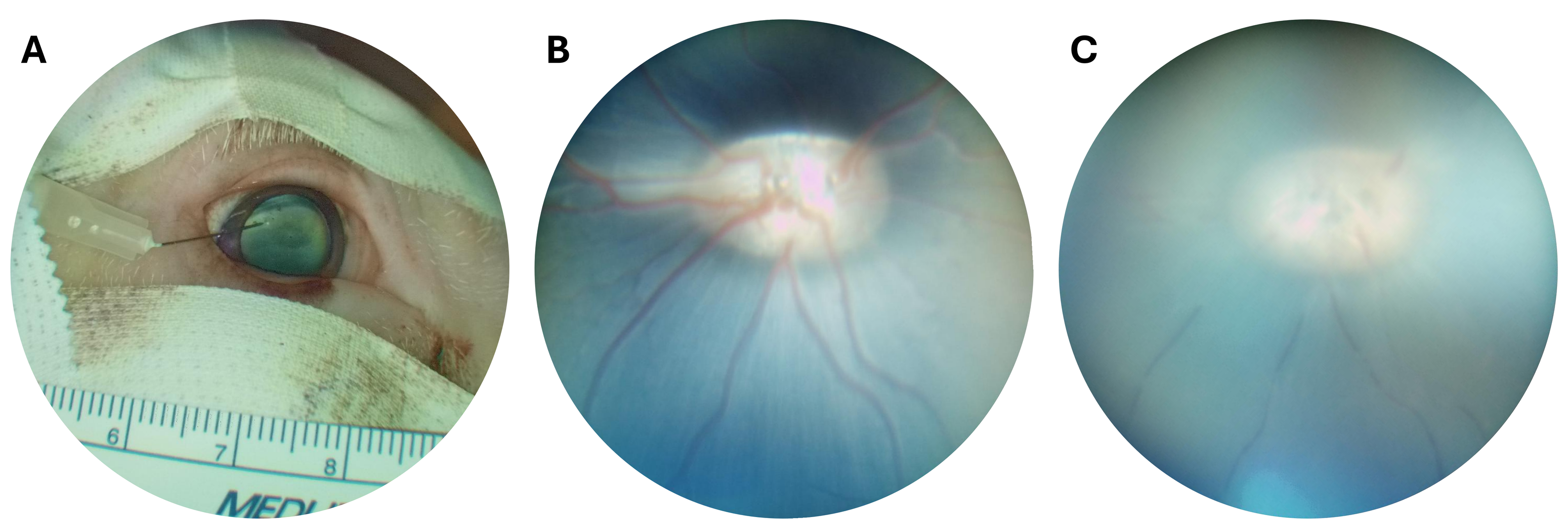

Fig. 2. Porcine acute traumatic ocular hypertension injury model. (A) A 30-gauge needle connected to an elevated saline bag is inserted into the anterior chamber via the limbus to elevate intraocular pressure to ~125 mmHg. (B) Fundus image before injury showing normal retinal vasculature and unobstructed blood flow to the optic nerve. (C) Fundus image during sustained pressure elevation showing blanching and loss of retinal blood flow, confirming induction of acute ocular hypertension.

DAY 0 — STEP 1	DAY 0 — STEP 2	DAY 0 — STEP 3	DAY 14 — ENDPOINT
Baseline	**Injury Induction**	**Immediately After**	**Study Conclusion**
RETImap: pERG + SLO	Fundus Imaging and Pressure Monitoring	RETImap: pERG + SLO and MBV Administration	RETImap + Necropsy → Histology

RESULTS

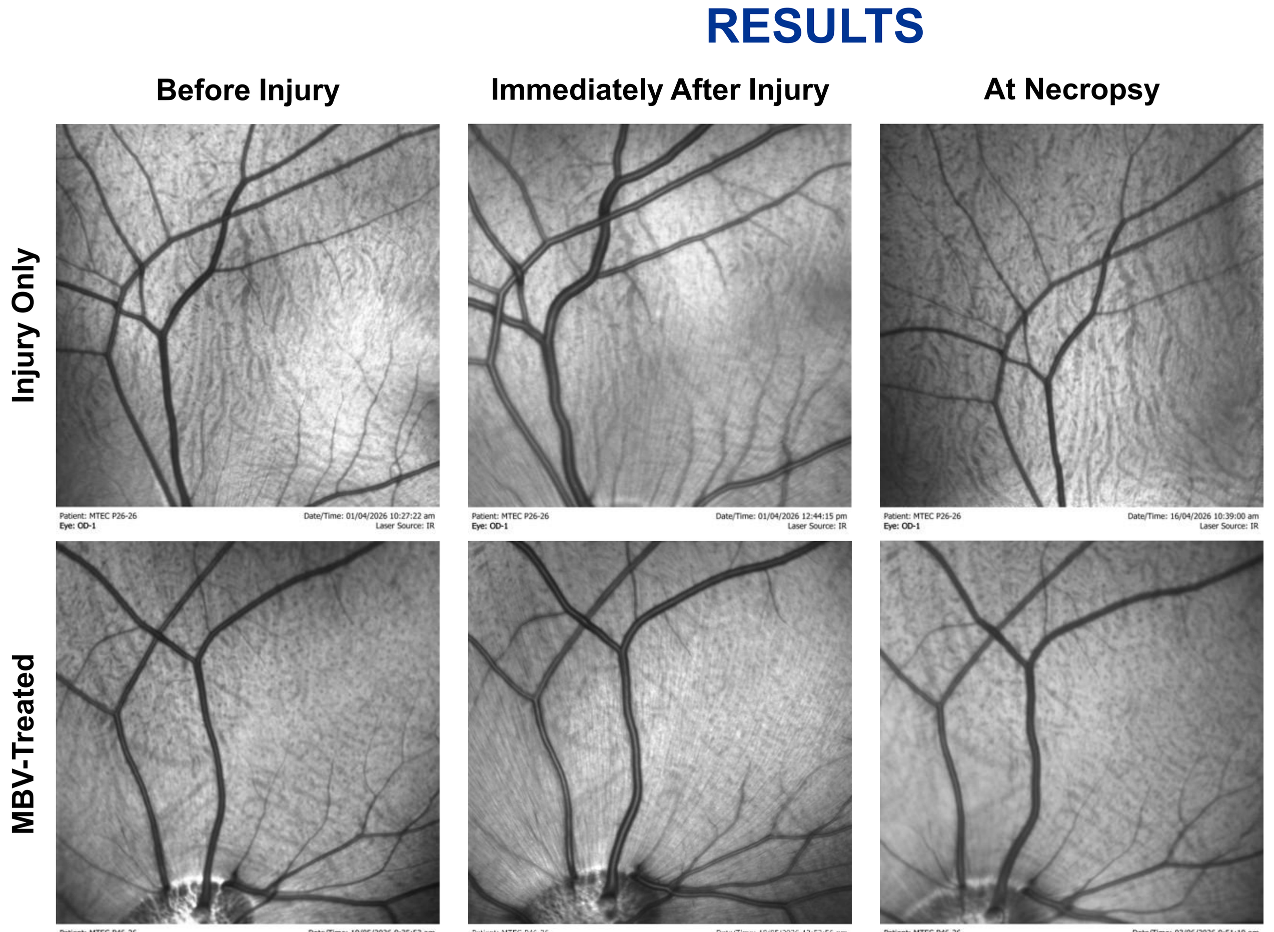

Fig. 3. Scanning laser ophthalmoscope images of the peripheral retinal vasculature. SLO fundus images before injury, immediately after injury, and at the 14-day study endpoint for injury-only and MBV-treated eyes. Vessel caliber visibly increased in both groups immediately after injury; by day 14, vessel appearance diverged between the two conditions (quantified in Fig. 5).

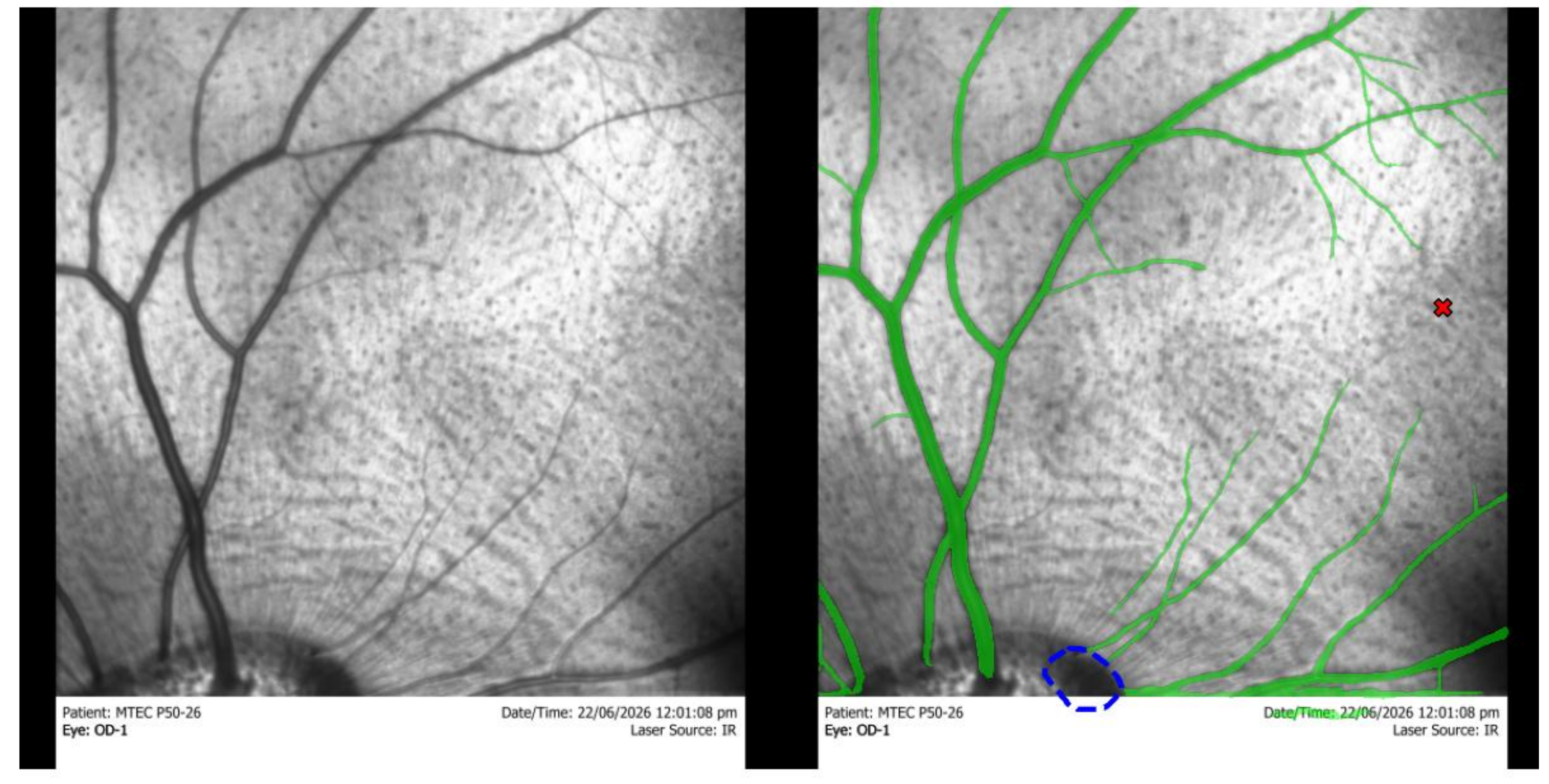

Fig. 4. Automated SLO vessel segmentation. Representative segmentation of the peripheral retinal vasculature (left, unprocessed SLO image; right, segmented vessels in green) using the open-source image-analysis toolkit SLOctolyzer (v1.0).

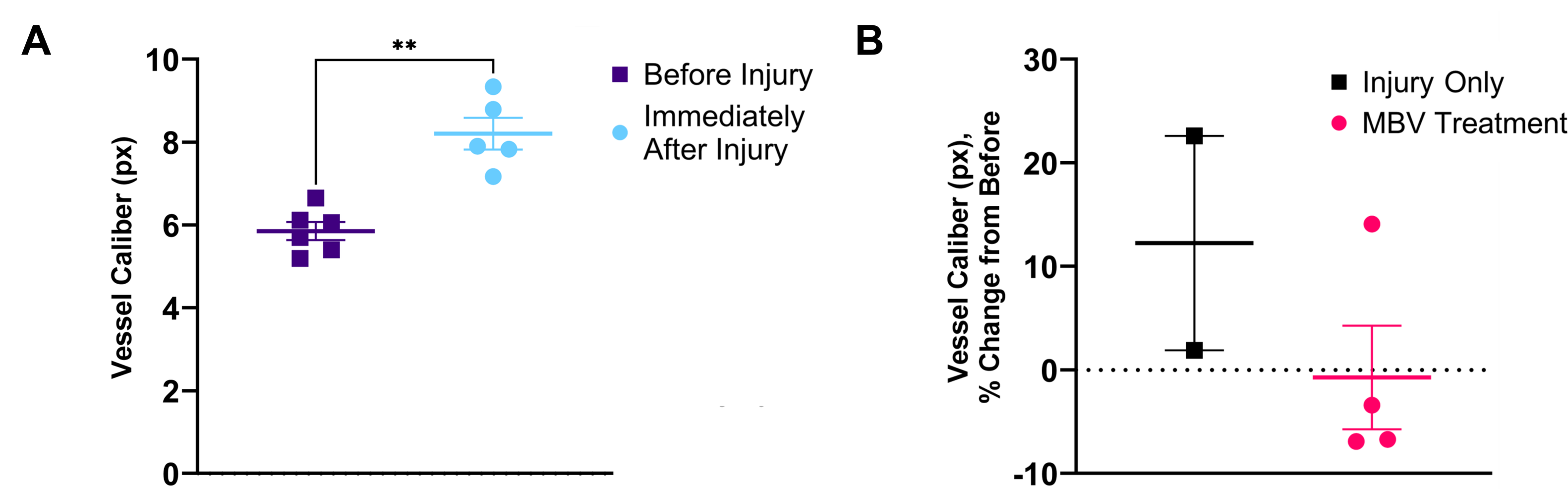

Fig. 5. Vessel caliber before and immediately after injury, and by treatment group at the 14-day endpoint. (A) Vessel caliber before injury (purple, n=6) and immediately after injury induction (blue, n=5), measured from SLO images. Asterisks (**) indicate p<0.01 (paired t-test). (B) Vessel caliber at the 14-day endpoint, expressed as percent change from pre-injury baseline (dotted line). Sample sizes were as follows: injury only (black, n=2), MBV treatment (pink, n=4). Individual data points are shown in both panels for each pig, with horizontal bars and error bars representing mean ± SEM.

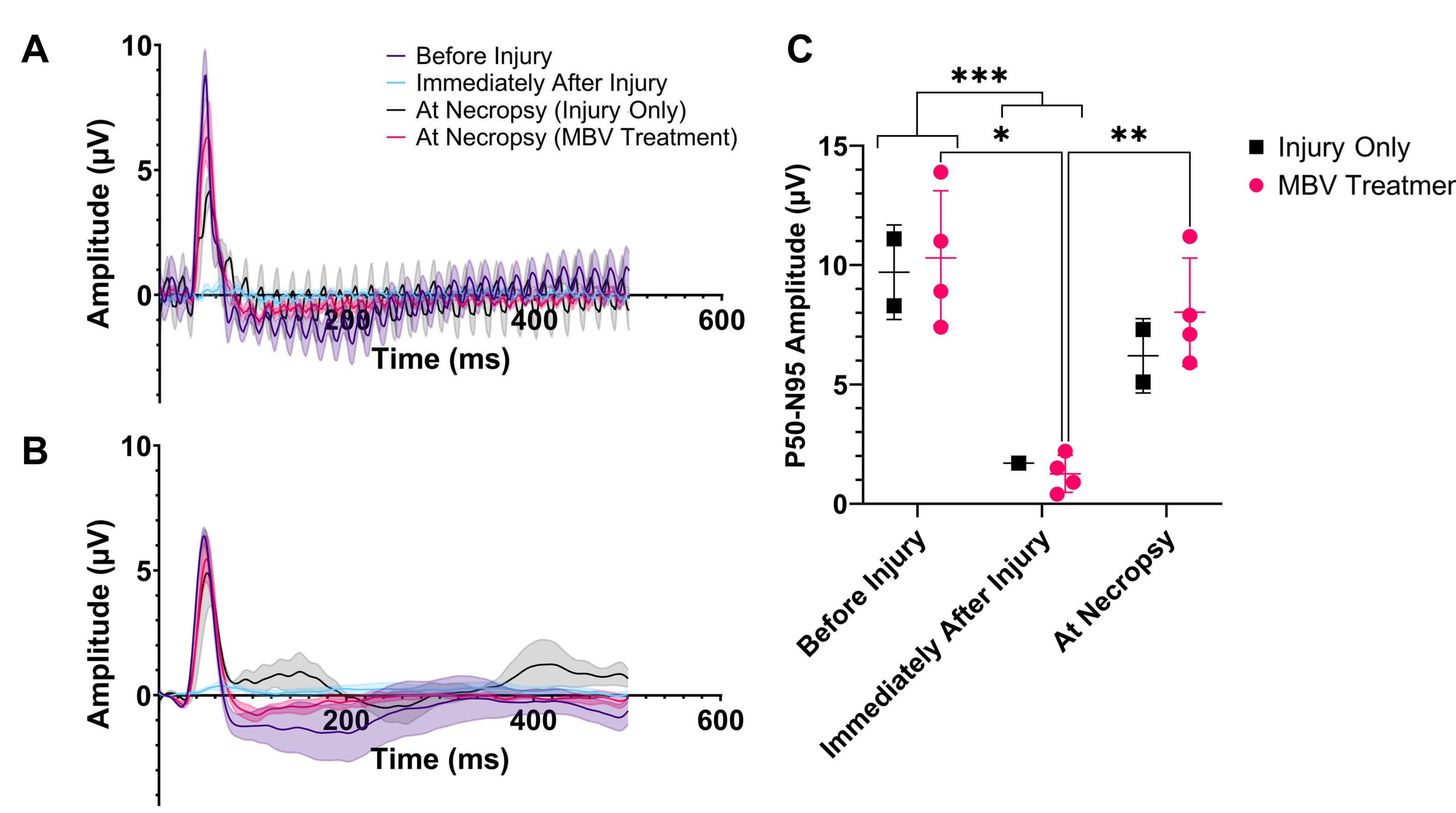

Fig. 6. Pattern ERG waveforms and P50-N95 amplitude, before injury through the 14-day endpoint. Average pERG waveforms, unfiltered (A) and bandpass filtered (B), before injury (purple), immediately after injury (blue), and at the 14-day endpoint for injury-only (black) and MBV-treated (pink) eyes. Shaded regions represent SEM. (C) P50-N95 amplitude for injury-only (black, n=2) and MBV-treated (pink, n=4) pigs at each timepoint. Significant differences within MBV-treated eyes across timepoints are indicated by *p<0.05 and **p<0.01 (mixed-effects model with Tukey's multiple comparisons test); the pooled comparison of both groups before vs. immediately after injury is indicated by ***p<0.001 (paired t-test). Individual data points are shown for each sample, with horizontal bars and error bars representing mean ± SEM.

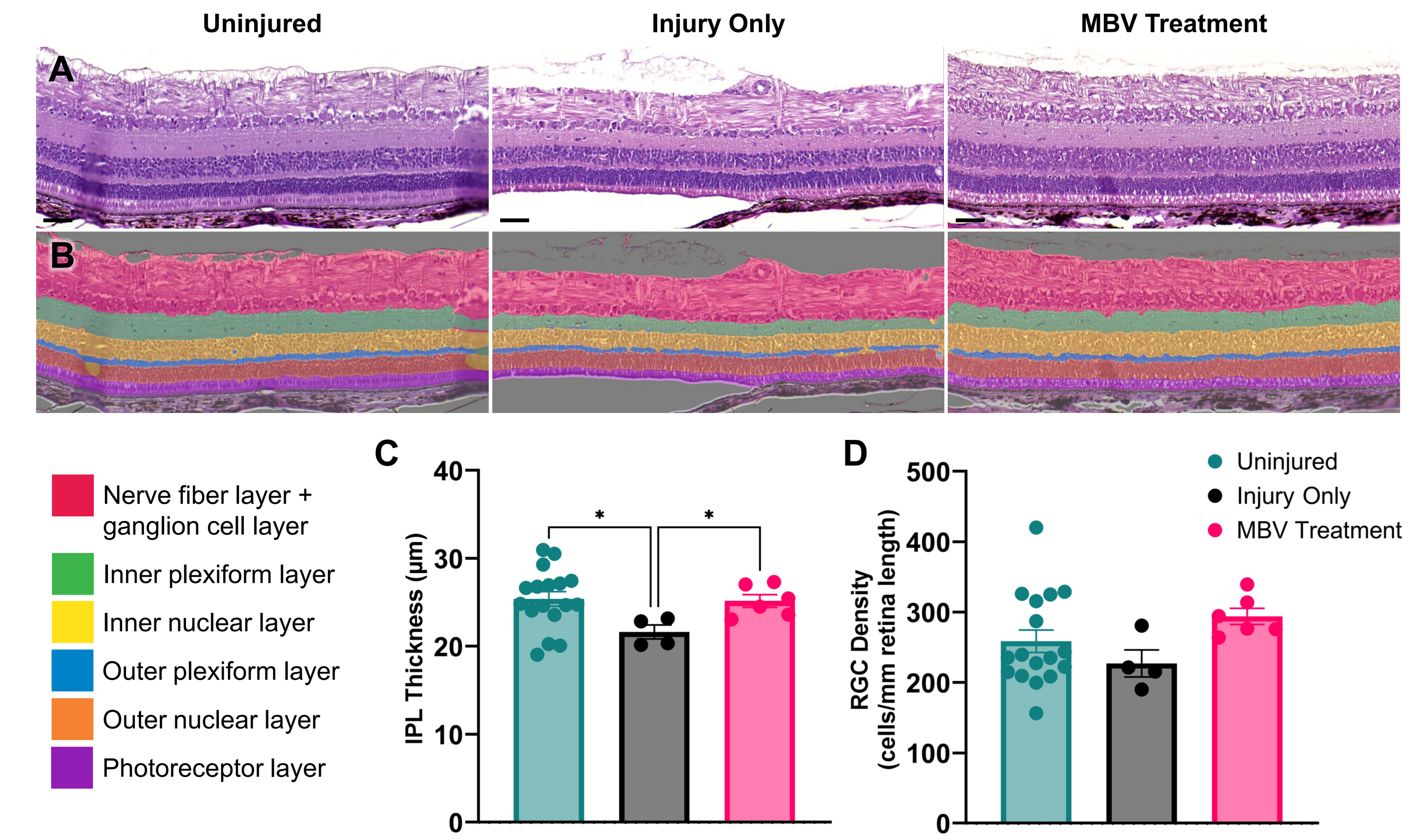

Fig. 7. Retinal architecture across injury and treatment groups. (A) Representative hematoxylin & eosin cross-sections of the retina for uninjured, injury-only, and MBV-treated eyes at 14 days. Scale bars 50 μm. (B) Automated segmentation overlay of the same sections into six retinal layers (nerve fiber layer + ganglion cell layer, inner plexiform layer, inner nuclear layer, outer plexiform layer, outer nuclear layer, photoreceptor layer), color-coded as shown in the legend. (C) Average inner plexiform layer (IPL) thickness for uninjured contralateral (teal, n=17), injury-only (black, n=4), and MBV-treated (pink, n=6) eyes. Individual data points are shown for each animal, with bars representing mean ± SEM. Asterisks (*) indicate pairwise comparisons with p<0.05 (Welch's ANOVA followed by Dunnett's T3 multiple comparisons test). (D) Retinal ganglion cell (RGC) density per eye, expressed as cells per mm of retina length. Same groups and sample sizes as in (C).

FUTURE DIRECTIONS

1. **Therapeutic Window:** Test delayed MBV administration to reflect realistic delays in treatment access during combat operations.
2. **Mechanistic Studies:** Expand immunohistochemistry characterization to clarify pathways of MBV-mediated protection.
3. **Longer-Term Follow-Up:** Assess structural and functional preservation beyond the 14-day endpoint.

CONCLUSIONS

This study establishes a reproducible porcine model of acute traumatic ocular hypertension, validated both structurally and functionally. Fundus and SLO imaging confirmed acute vascular changes consistent with injury, and pattern ERG confirmed a corresponding loss of retinal function. Beyond this specific therapy, the model itself represents a translatable platform for evaluating future field-deployable treatments against this combat-relevant injury. MBV treatment was associated with meaningful preservation of retinal structure and function. Inner plexiform layer thickness in MBV-treated eyes did not differ significantly from uninjured controls and was significantly greater than in injury-only eyes, and pERG amplitude in MBV-treated eyes recovered to significantly higher levels by the 14-day endpoint relative to immediately after injury. Vessel caliber and retinal ganglion cell density showed encouraging trends toward preservation with MBV treatment, though these did not reach statistical significance given the small sample sizes evaluated to date. Together, these findings support continued investigation of MBV as a portable, off-the-shelf, field-deployable therapy to minimize secondary injury and preserve vision after combat-related ocular trauma.

ACKNOWLEDGEMENTS

We thank the University of Pittsburgh's McGowan Institute Histology Core Laboratory and the Bridgeside Point II DLAR facility for supporting the histology services and animal care essential to this study.

This study was funded by the Medical Technology Enterprise Consortium (MTEC), Research Project Number MTEC-23-06-USAMRDC-MultiTopic-122.

MTEC Medical Technology Enterprise Consortium